Annals of Nuclear Energy 43 (2012) 31–38

Contents lists available at SciVerse ScienceDirect

Annals of Nuclear Energy

journal homepage: www.elsevier.com/locate/anucene

Application of the wavelet expansion method in spatial-angular discretization of the neutron transport equation

Youqi Zheng *, Hongchun Wu, Liangzhi Cao

School of Nuclear Science and Technology, Xi'an Jiaotong University, Xi'an, Shaanxi 710049, China

ARTICLE INFO

Article history:
Received 2 June 2011
Received in revised form 20 September 2011
Accepted 11 December 2011
Available online 20 January 2012

Keywords:
Neutron transport equation
Daubechies wavelets
Angular discretization
Spatial discretization

ABSTRACT

This paper describes the wavelet expansion method for discretizing the angular and spatial variables in the neutron transport equation. Three special features are introduced: (a) the variation scheme is applied using the Daubechies scaling function as the trialing and weighting functions, (b) the corresponding expansion sequence is designed for the sweeping of nodes, and (c) the boundary conditions and interface conditions are expressed using the wavelet expansion. The numerical results of several benchmarks demonstrate that the new method is feasible for the spatial-angular discretization of neutron transport equation. It is accurate and suitable for solving the problems with large flux gradient.

1. Introduction

Many numerical methods have been developed to solve the neutron transport equation in past decades, such as the finite difference method (FDM), the finite element method (FEM) and the nodal method (Lewis and Miller, 1984). In this paper, we introduce a new method called the wavelet expansion method (WEM) to solve the first-order neutron transport equation. In this method, the flux distribution is represented by the wavelet expansion and the Daubechies scaling functions are adopted as the basis function.

The wavelets are well developed in recent years and widely used in the fields of science and engineering. Daubechies (1992) constructed a kind of wavelets based on the multi-resolution analysis (MRA) theory and named them 'the Daubechies wavelets'. These wavelets possess the properties of orthonormality and compact support. Cho and Park (1996) introduced them in solving the neutron diffusion equation. Nasif et al. (1999, 2001) improved it by using a new method to generate the connection coefficients and the boundary condition. The wavelets were first introduced into solving the neutron transport equation by Carron (1999) for the angular discretization. Buchan et al. (2008a,b) developed this approach further and proposed a second generation type wavelet expansion for the angular discretization.

The Daubechies wavelets were initially introduced into discretizing the angular variables of neutron transport equation by Cho and Cao (2006). Zheng et al. (2009, 2010) improved it by applying the Daubechies scaling function on the interval (Cohen et al., 1993) as the basis function and proposed the decoupled angular discretization scheme. Yang et al. (2010) introduced the Daubechies wavelets into the resonance self-shielding calculation. Previous studies indicated that the WEM method is advanced and attractive. It possesses higher accuracy and can well handle the problems suffering large graded distribution.

In this paper, the wavelet expansion method is extended to discretize both the angular and spatial variables. For the angular discretization, the same approaches are referred directly from previous works. For the spatial discretization, new approaches are proposed. The variation method is applied. The boundary conditions and interface conditions are expressed using the wavelet expansion. A sweeping scheme is proposed and the corresponding sequence is appointed to determine the order that the wavelet coefficients are solved. Several test problems are calculated to demonstrate the accuracy and advantages of the new method.

In Section 2, the fundamentals of Daubechies wavelets and their application in the angular discretization is reviewed. The spatial discretizing process is presented in Section 3. The test results are shown in Section 4 to demonstrate the effectiveness and accuracy of the new method. Finally, Section 5 provides the conclusions to close the paper.

2. Wavelet expansion in the angular domain

This paper uses the same angular discretization scheme as in previous works (Zheng et al., 2009, 2010). To avoid duplication, the detailed explanation is omitted in this paper. Some useful

* Corresponding author. Tel.: +86 29 8266 3285; fax: +86 29 8266 7802.
E-mail address: yqzheng@mail.xjtu.edu.cn (Y. Zheng).

0306-4549/$ - see front matter © 2011 Elsevier Ltd. All rights reserved.
doi:10.1016/j.anucene.2011.12.018

properties and process applicable to this paper's content are reviewed in this section.

2.1. Review of the Daubechies wavelets

The Daubechies wavelets (Daubechies, 1992) consist of the Daubechies scaling function and wavelet function. In this paper, only the Daubechies scaling function is used as the basis function, which can be represented as:

$$\psi_{n,k}(x) = 2^{n/2}\psi(2^n x - k) \tag{1}$$

The Daubechies wavelets are orthonormal and compactly supported as:

$$\psi_{n,k}(x) = \sum_{j=2k}^{2N+2k-1} c_{j-2k}\psi_{n+1,j}(x), \text{support } (\psi_{n,k}) = [2^{-n}k, 2^{-n}(k+2N-1)] \tag{2}$$

and

$$\int \psi_{n,k}(x)\psi_{n,l}(x)dx = \delta_{kl} \tag{3}$$

Here, N is the Daubechies order, n is the dilation order and also the expansion order used in the latter sections. The coefficients c are called the Daubechies coefficients (1992). Fig. 1 shows the scaling functions with different Daubechies order. In order to generate the derivative of wavelets, the scaling function with higher

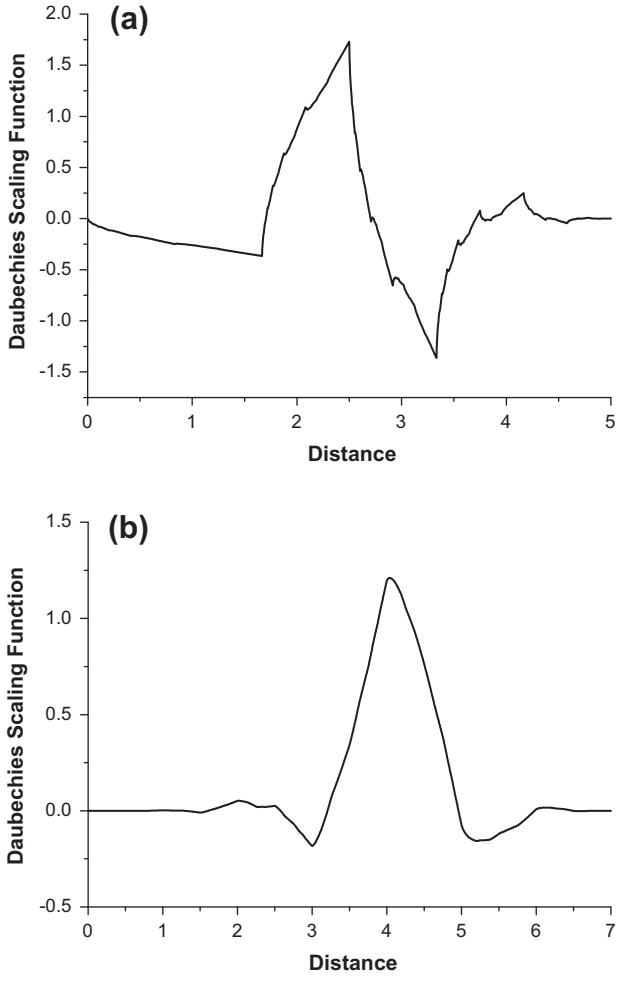

Fig. 1. Distribution of the Daubechies scaling function (a) for $N = 2$ (b) for $N = 4$.

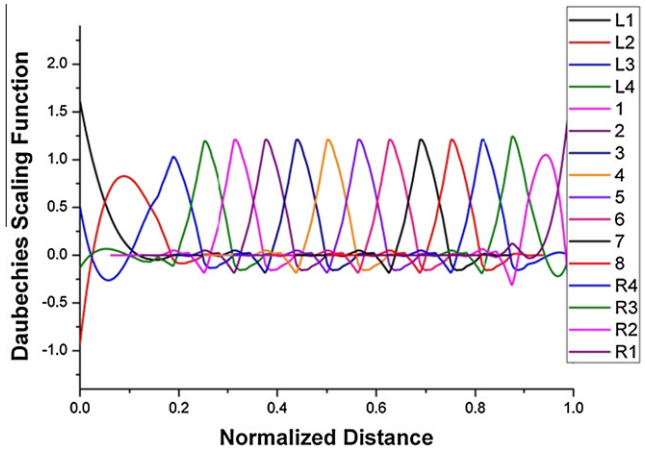

Fig. 2. Distribution of the Daubechies scaling function series on the interval ($N = 4$). (For interpretation of the references to colour in this figure legend, the reader is referred to the web version of this article.)

Daubechies order is used for its better continuity. The wavelets on the interval are used to avoid the 'edge effect' (Zheng et al., 2009, 2010) and get accurate simulation near the boundary or interface. Fig. 2 indicates the distribution of wavelets on the normalized interval.

According to Eq. (1), the Daubechies scaling function has no explicit expression. The discrete values are obtained by the numerical method. Using the definition in Eqs. (1) and (3), the values of scaling functions at the integer points are generated as (taking $N = 2$ for example, $\psi(0) = \psi(3) = 0$ for the property of compact support):

$$\psi(1) = c_1\psi(1) + c_0\psi(2) \tag{4a}$$

$$\psi(2) = c_3\psi(1) + c_2\psi(2) \tag{4b}$$

An iterative method is applied to solve Eq. (4). The values at 1/2 can be obtained using Eq. (2). Then, other values at 1/4, 1/8 and $1/2^n$ are obtained in the same way recursively.

2.2. Decoupled angular discretization

A decoupled angular discretization scheme has been proposed (Zheng et al., 2009, 2010). The angular domain is divided into several sub-domains as shown in Fig. 3. The polar and azimuthal variables are discretized separately in each sub-domain.

The two-dimensional multi-group neutron transport equation is:

$$\Omega_x \frac{\partial \phi_g(r,\Omega)}{\partial x} + \Omega_y \frac{\partial \phi_g(r,\Omega)}{\partial y} + \Sigma_{t,g}\phi_g(r,\Omega) = q_g(r,\Omega) \tag{5}$$

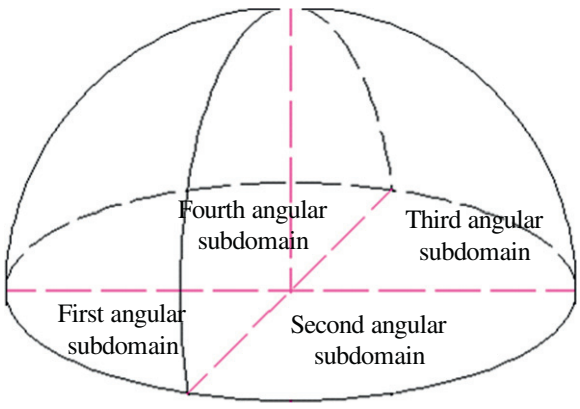

Fig. 3. Definition of angular subdomains in the X–Y geometry.

where ϕ is the flux and q is the source distribution. In this paper, only the X–Y geometry is considered. Thus,

$$\Omega_x = (1-\mu^2)^{1/2}\cos\varphi \tag{6a}$$

$$\Omega_y = (1-\mu^2)^{1/2}\sin\varphi \tag{6b}$$

where μ is the cosine of polar variable and ϕ is the azimuthal variable.

The polar variable is discretized using the discrete ordinate method as:

$$\int_{\Delta\mu_m}\left\{\Omega_x\frac{\partial\phi_g(r,\Omega)}{\partial x}+\Omega_y\frac{\partial\phi_g(r,\Omega)}{\partial y}+\Sigma_{t,g}\phi_g(r,\Omega)-q_g(r,\Omega)\right\}d\mu = 0 \tag{7}$$

And the discretized form can be written as:

$$\sqrt{1-\mu_m^2}\cos\varphi\frac{\partial\phi_{g,m}(r,\varphi)}{\partial x}+\sqrt{1-\mu_m^2}\sin\varphi\frac{\partial\phi_{g,m}(r,\varphi)}{\partial y}+\Sigma_{t,g}\phi_{g,m}(r,\varphi)=q_{g,m}(r,\varphi) \tag{8}$$

where

$$\int_{\Delta\mu_m}\phi_g(r,\Omega)d\mu=\omega_m\phi_{g,m}(r,\varphi) \tag{9}$$

The azimuthal variable is expanded by the Daubechies scaling function as:

$$\phi_{g,m}(r,\varphi)=\sum_{p=1}^{np}\phi_{g,mp}(r)\psi_p(\xi),\quad \xi=\frac{2}{\pi}\varphi,\ \text{and}\ \xi\in[0,1) \tag{10}$$

Finally, the angularly discretized equation is obtained as:

$$\sum_{p=1}^{np}\left(a^kD_{x,mpp'}\frac{\partial\phi^k_{g,mp}}{\partial x}+b^iD_{y,mpp'}\frac{\partial\phi^k_{g,mp}}{\partial y}\right)+\Sigma_{t,g}\phi^k_{g,mp'}=q^k_{g,mp'},\ \ p'=1,np \tag{11}$$

where k is the index of angular sub-domain, a^k and b^k are appointed as:

$$a^1=-1,\quad a^2=1,\quad a^3=1,\quad a^4=-1 \tag{12}$$

$$b^1=-1,\quad b^2=-1,\quad b^3=1,\quad b^4=1 \tag{13}$$

and the coefficients are defined as:

$$D_{x,mpp'}=\sqrt{1-\mu_m^2}\int\cos\frac{\pi}{2}\xi\psi_p(\xi)\psi_{p'}(\xi)d\xi \tag{14}$$

$$D_{y,mpp'}=\sqrt{1-\mu_m^2}\int\sin\frac{\pi}{2}\xi\psi_p(\xi)\psi_{p'}(\xi)d\xi \tag{15}$$

$$q_{g,mp'}=\int_0^1\psi_{p'}(\xi)S_{g,m}(r,\xi)d\xi \tag{16}$$

The integrations in Eqs. (14)–(16) are calculated using the trapezoidal method.

3. Wavelet expansion in the spatial domain

The spatial discretization scheme is deduced in this section. Since the angularly discretized equations as in Eq. (11) are coupled by a series of coefficients $\phi^k_{g,mp}$, the iterative method is applied to decouple the coefficients as:

$$a^kD_{x,mpp'}\frac{\partial\phi^{k,l}_{g,mp'}}{\partial x}+b^iD_{y,mpp'}\frac{\partial\phi^{k,l}_{g,mp'}}{\partial y}+\Sigma_t\phi^{k,l}_{g,mp'}=q^{k,l-1}_{g,mp'}-\sum_{p=1,p\neq p'}^{np}\left(a^kD_{x,mpp'}\frac{\partial\phi^{k,l-1}_{g,mp}}{\partial x}+b^kD_{y,mpp'}\frac{\partial\phi^{k,l-1}_{g,mp}}{\partial y}\right)=q'^{k,l-1}_{g,mp'}\quad p'=1,np \tag{17}$$

where l denotes the iteration index.

3.1. Variation of the neutron transport equation

The variation method is used on the nodes as in Fig. 4. In the variation process, the weighting function ϕ^0 is multiplied on both sides of Eq. (17). Then, the integration is done as:

$$\int_{a_y}^{b_y}\int_{a_x}^{b_x}\left(a^kD_{x,mp'p'}\frac{\partial\phi^k_{g,mp'}}{\partial x}+b^kD_{y,mp'p'}\frac{\partial\phi^k_{g,mp'}}{\partial y}+\Sigma_{t,g}\phi^k_{g,mp'}-q^k_{g,mp'}\right)\phi^0dxdy=0,\ \ p'=1,np \tag{18}$$

In this paper, the trialing and weighting functions are both the Daubechies scaling functions in the tensor product form as:

$$\phi^k_{g,mp'}(x,y)=\sum_{i=1}^{npi}\sum_{j=1}^{npj}\phi^k_{g,mp',ij}\psi_i(x)\psi_j(y) \tag{19}$$

$$\phi^0(x,y)=\psi_{i'}(x)\psi_{j'}(y) \tag{20}$$

where npi and npj are the total number of expansion coefficients, determined by the expansion order in the X- and Y-dimension, respectively.

3.2. Deduction of the spatial discretization

Generally, a given node should be transferred into the normalized node first. The normalized variables are expanded by the Daubechies scaling functions as:

$$\int_0^1\int_0^1\sum_{i=1}^{npi}\sum_{j=1}^{npj}\left(a^iD_{x,mp'p'}\phi^k_{g,mp',ij}\psi_j(\xi_y)\frac{d\psi_i(\xi_x)}{d\xi_x}+b^iD_{y,mp'p'}\phi^k_{g,mp',ij}\psi_i(\xi_x)\frac{d\psi_j(\xi_y)}{d\xi_y}+\Sigma_t\phi^k_{g,mp',ij}\psi_i(\xi_x)\psi_j(\xi_y)-q'^k_{g,mp'}\right)\times\psi_{i'}(\xi_x)\psi_{j'}(\xi_y)|J(\xi_x,\xi_y)|d\xi_xd\xi_y=0,\quad i'=1,npi;\ j'=1,npj;\quad p'=1,np \tag{21}$$

where $|J(\xi_x,\xi_y)|$ is the Jacobian matrix, defined as:

$$|J(\xi_x,\xi_y)|=\begin{vmatrix}\frac{\partial x}{\partial\xi_x} & \frac{\partial y}{\partial\xi_x}\\ \frac{\partial x}{\partial\xi_y} & \frac{\partial y}{\partial\xi_y}\end{vmatrix} \tag{22}$$

Considering the orthonormality of Daubechies scaling function, the variation can be simplified as:

$$a^k\Delta yD_{x,mp'p'}\sum_{i=1}^{npi}\phi^k_{g,mp',ij'}\int_0^1\frac{d\psi_i(\xi_x)}{d\xi_x}\psi_{i'}(\xi_x)d\xi_x+b^k\Delta x\sum_{j=1}^{npj}D_{y,mp'p'}\phi^k_{g,mp',i'j}\int_0^1\frac{d\psi_j(\xi_y)}{d\xi_y}\psi_{j'}(\xi_y)d\xi_y+\Sigma_t\phi_{g,mp',i'j'}\Delta x\Delta y=q'^k_{g,mp'}\Delta x\Delta y\int_0^1\psi_{i'}(\xi_x)d\xi_x\int_0^1\psi_{j'}(\xi_y)d\xi_y,\quad i'=1,npi;\ j'=1,npj;\ p'=1,np \tag{23}$$

where Δx and Δy denote the size of original nodes. The derivative of Daubechies scaling function is calculated using:

$$\left.\frac{d\psi_i(\xi_x)}{d\xi_x}\right|_{\xi_x=x_0}=\frac{\psi_i(x_0+d/2^{n+1})-\psi_i(x_0-d/2^{n+1})}{d/2^n} \tag{24a}$$

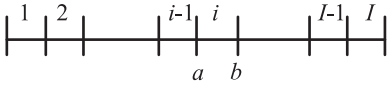

Fig. 4. Configuration of the slab geometry.

and

$$\left.\frac{d\psi_j(\xi_y)}{d\xi_y}\right|_{\xi_y=y_0} = \frac{\psi_j(y_0+d/2^{n+1})-\psi_j(y_0-d/2^{n+1})}{d/2^n} \tag{24b}$$

With all the coefficients in Eq. (23) known, the wavelet expansion coefficients can be obtained by solving the matrix:

$$K\psi = b \tag{25}$$

where,

$$K_{i,j} = a^k \Delta y D_{x,mp'p'} C_{x,ii'} \phi^k_{g,mp',ij'} + b^k \Delta y D_{x,mp'p'} C_{y,jj'} \phi^k_{g,mp',i'j} + \begin{cases} \Sigma_{t,g}\phi^k_{g,mp',i'j'}\Delta x\Delta y, & i=i',\ j=j' \\ 0, & \text{else} \end{cases} \tag{26}$$

$$\psi = [\phi^k_{g,mp',11}, \phi^k_{g,mp',21}, \ldots, \phi^k_{g,mp',npinpj}]^T \tag{27}$$

and

$$b = [E_{11}q'^k_{g,mp'}, E_{21}q'^k_{g,mp'}, \ldots, E_{npinpj}q'^k_{g,mp'}]^T \tag{28}$$

with,

$$C_{x,ii'} = \Delta y \int_0^1 \frac{d\psi_i(\xi_x)}{d\xi_x}\psi_{i'}(\xi_x)d\xi_x \text{ and } C_{y,jj'} = \Delta x \int_0^1 \frac{d\psi_j(\xi_y)}{d\xi_y}\psi_{j'}(\xi_y)d\xi_y \tag{29}$$

$$E_{ij} = \Delta x\Delta y \int_0^1 \psi_i(\xi_x)d\xi_x \int_0^1 \psi_j(\xi_y)d\xi_y \tag{30}$$

3.3. Boundary condition in the wavelet expansion form

In this paper, two typical boundary conditions are considered:
(i) The reflective boundary condition, which is defined as:

$$\phi_g(r_b,\Omega) = \phi_g(r_b,\Omega'),\ \Omega\cdot n<0 \tag{31}$$

where Ω' is the reflective angle of Ω. For the angular discretization, the boundary condition is given as:

$$\phi^k_{g,mp}(x,y) = \phi^{k^{ref}}_{g,mp}(x,y), \quad p=1,np \tag{32}$$

After expanding the spatial variables, the boundary condition is transformed to be:

$$\sum_i\sum_j \phi^k_{g,mp,ij}\psi_i(0)\psi_j(y) = \sum_{i'}\sum_{j'} \phi^{k^{ref}}_{g,mp,i'j'}\psi_{i'}(0)\psi_{j'}(y) \tag{33}$$

Here, the left boundary is taken for instance.

Since the basis functions are not fully symmetric, it may lead the flux simulation in the spatial domain to be distorted in the sweeping of nodes. Especially in the two-dimensional calculation, this phenomenon sometimes induces the divergence of iteration. To avoid it, the corresponding expansion sequence is designed as in Table 1.

Table 1
Expansion sequence in the quadrant.

Quadrant	Expansion sequence	
	X-dimension	*Y*-dimension
1	*i* = 1,*npi*	*j* = *npj*,1
2	*i* = 1,*npi*	*j* = 1,*npj*
3	*i* = *npi*,1	*j* = *npj*,1
4	*i* = *npi*,1	*j* = 1,*npj*

Based on the expansion sequence, the boundary condition is finally represented as:

$$\sum_i \phi^k_{g,mp,ij}\psi_i(0) = \sum_{i'} \phi^{k^{ref}}_{g,mp,i'j'}\psi_{i'}(0)\sum_{j'}\psi_{j'}(\xi_y)\int_0^1 \psi_{j'}(\xi_y)\psi_j(\xi_y)d\xi_y \tag{34}$$

where j is determined as in Table 1. The trapezoidal method is used here to calculate the integrations.

(ii) The vacuum boundary condition, which is defined as:

$$\phi_g(r_b,\Omega) = 0,\ \Omega\cdot n<0 \tag{35}$$

Using similar treatments, the boundary condition is finally transformed as:

$$\sum_i \phi^k_{g,mp,ij}\psi_i(0) = 0 \tag{36}$$

where j is the same with the one in Eq. (34).

The wavelet expansion coefficients are calculated node by node as illustrated in Fig. 5. The interface condition should be determined to make the flux continuous along the sweeping direction as:

$$\phi_g(r_i,\Omega) = \phi_g(r_{i-1},\Omega) \tag{37}$$

where r_i and r_{i-1} denote the interface for node (i,j) and $(i-1,j)$, respectively. The same treatments are applied to generate the interface condition, and finally it is rewritten as:

$$\sum_i \phi^k_{g,mp,ij}\psi_i(0) = \sum_{i'} \phi^k_{g,mp,i'j'}\psi_{i'}(1)\sum_{j'}\psi_{j'}(\xi_y) \times \int_0^1 \psi_{j'}(\xi_y)\psi_j(\xi_y)d\xi_y \tag{38}$$

where the left side of node (i,j) is taken for instance and j is also determined as in Table 1.

Combining the boundary condition and interface condition with the matrix required the replacement of some original equations. In this paper, we select the equations at the beginning or ending line in every block of the matrix. For the right and top sides, the ending line is replaced while the beginning one is replaced for the left and bottom sides. The modification is generally illustrated in Fig. 6. The Doolittle method is used to solve the matrix.

4. Numerical results

To find the capability of wavelet expansion method (WEM) in the angular and spatial discretization, several test problems are calculated in this section. All the calculations in this paper are carried out by PC (Intel Core2 Duo CPU E6750, 2.66 GHz, 2G memories).

4.1. Issa problem

This is a one-dimensional eigenvalue problem with core and shield regions (Issa et al., 1986). The cross section and geometry description are given in Fig. 7. The results are compared with the reference from ANISN using S_{16} approximation (Engle, 1973). Table 2 shows the results of eigenvalue (K_{eff}). For the angular variable, the expansion order is $n=4$, i.e. 16 unknowns in a quadrant are used. For further comparison, the results of finite difference method (FDM) with the same angular discretization are employed in this paper. Solutions using different expansion order in the spatial discretization are compared.

As in Table 2, the result from low order spatial expansion is accurate enough for this problem. Higher order can further improve the results, however, significantly reduce the efficiency. Fig. 8 illustrates the comparison of flux distribution in the medium. In the

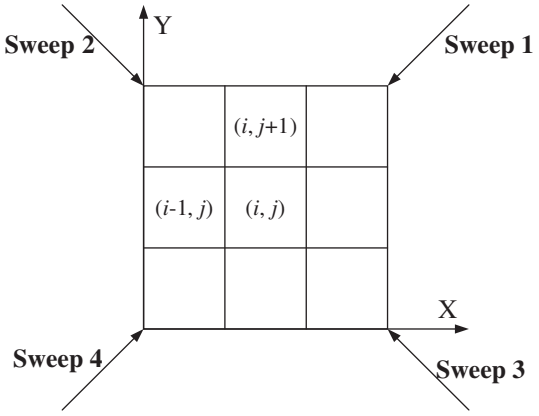

Fig. 5. Sweeping sequence of the nodes.

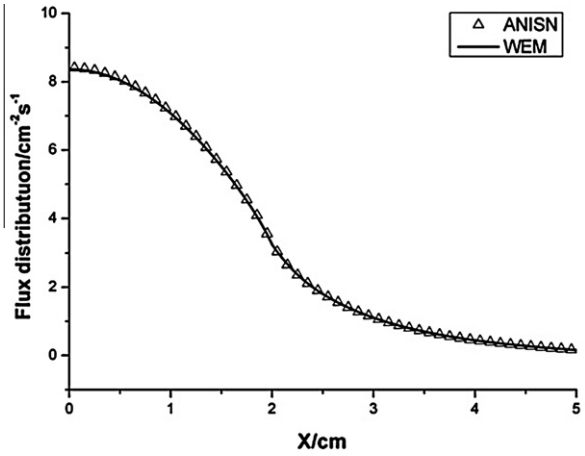

Fig. 8. Comparison of the flux distribution in Issa problem.

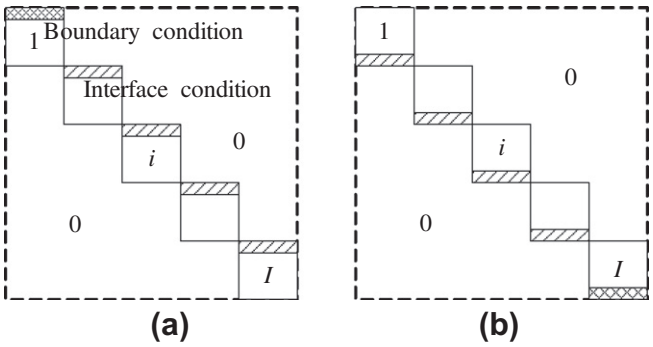

Fig. 6. The modification of matrix for the combination of boundary and interface condition (a) for the left and bottom sides (b) for the right and top sides.

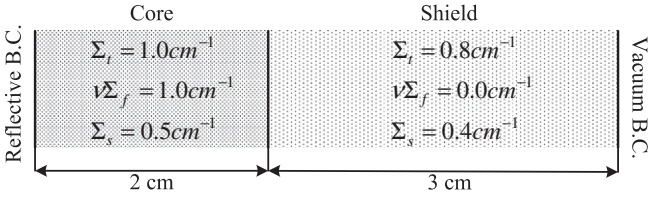

Fig. 7. Description of the Issa problem.

WEM method, the flux distribution is expressed in the continuous form rather than the discrete values in meshes. In the comparison, the calculated flux distribution agrees well with the reference.

4.2. Reed cell problem

This is a fixed source problem with five different regions (Buchan et al., 2005). It is calculated to test the capability of spatial wavelet expansion in handling the problems with large flux gradient. Fig. 9 illustrates the geometry and cross section of the problem. Since pure absorption, vacuum and strong scattering regions are all considered in this problem, the flux exhibits strong heterogeneous.

Fig. 10 illustrates the flux distribution in different regions. The angular expansion order is $n = 3$ (8 angular unknowns in each quadrant) and the FDM calculation is done to provide the reference results. In the FDM calculation, 80 and 400 meshes are used, respectively. It shows that the large gradient of flux distribution requires very fine mesh division, while the result from coarse mesh division suffers obviously distortion as illustrated in Fig. 10.

In the spatial wavelet expansion solution, five nodes are divided according to the five regions. Different expansion order is appointed in different regions. The expansion order $n = 4$ (16 unknowns in a node) is used in the second region and $n = 3$ (8 unknowns in a node) is used in others. Totally, 48 unknowns should be calculated. Compared with the FDM method, the WEM method performs better. No visual distortion can be viewed in the simulation. Compared with the fine mesh FDM method, the WEM method costs only a half of the computational time (0.92 s for the WEM calculation and 2.5 s for the fine mesh FDM calculation).

4.3. Simplified reactor core problem

This is a two-dimensional eigenvalue problem derived from a simplified reactor core. It is designed to test the feasibility and accuracy of wavelet expansion in the two-dimensional calculation. Four homogenized fuel assemblies compose the active region with the water reflector surrounded as in Fig. 11. Two-group cross section is given in Table 3.

The results including the K_{eff} and flux are given in Table 4. The reference results are calculated by the FDM method using the same angular discretization. The spatial expansion order used in this problem is $n = 3$ (8×8 unknowns in each of the nine nodes) and the reference solution uses 51×51 meshes. Fig. 12 illustrates the flux distribution along the bottom sides. Comparisons in Table 4 and Fig. 12 demonstrate that the WEM method can be used in

Table 2
Comparison of the eigenvalue of Issa problem.

	Reference	Wavelet expansion order		Total number of meshes in FDM	
		$n = 3$[a]	$n = 4$	25	50
K_{eff}	1.6784	1.6783	1.6784	1.6780	1.6781
Error/%	–	−0.006	−0.001	−0.024	−0.018
CPU time/s	–	2.9	34.4	0.5	1.9

[a] The number of unknowns is 2^n, i.e. 8 for $n = 3$ and 16 for $n = 4$ in each node.

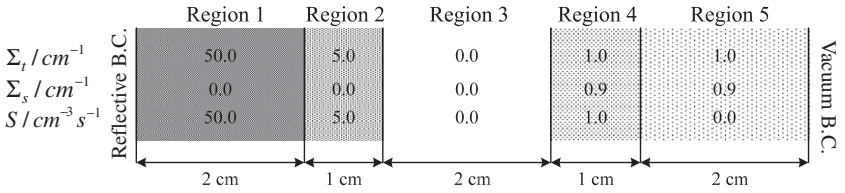

Fig. 9. Description of the Reed cell problem.

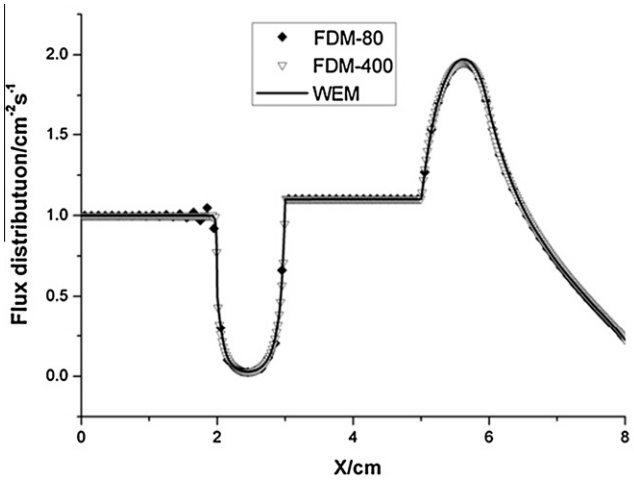

Fig. 10. Comparison of the flux distribution of Reed cell problem.

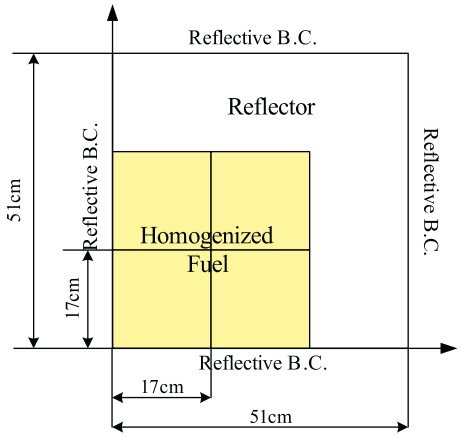

Fig. 11. Geometry of the simplified reactor core problem.

the two-dimensional calculation. Both the K_{eff} and flux are accurate enough. However, the CPU time cost is larger than the FDM method in this problem.

4.4. Deep penetration problem

This is a two-dimensional fixed source problem derived from the neutron detection process. In the optical thick medium, the neutron flux decreases sharply at the interface of source zone and medium zone, i.e. large gradient arises. The descriptions of geometry and cross section are given in Fig. 13 and Table 5, respectively. The reference results are calculated using the FDM method with the same angular discretization.

Fig. 14 illustrates the flux distribution along the *X*-direction. The reference results are obtained by using 18,620 meshes and cost 27.6 s. In the wavelet expansion method, the medium is divided by 4×4 nodes. In each node, the expansion order is $n = 3$ and totally 1024 unknowns need to be determined. As in Fig. 14, both the fast flux and thermal flux decrease sharply in the medium. The wavelets reconstruct such distribution precisely. However, the CPU time cost is 60.6 s, which is also larger than the one FDM costs.

5. Conclusion

In this paper, a new method using the wavelet expansion to discretize the angular and spatial variables in the neutron transport equation is described. The angular variable is discretized using the decoupled scheme. The tensor product spatial expansion is applied in the two-dimensional calculations, in which the basis function is also the Daubechies scaling function. A sweeping scheme is designed together with the appointed expansion sequence to avoid the effect of asymmetric basis function. The boundary conditions and interface conditions are all expressed using the wavelet expansion and added into the matrix originally generated from the variation scheme.

Table 3
Cross section of the simplified rector core problem.

		$\nu\Sigma_f$ (cm^{-1})	Σ_{1-1} (cm^{-1})	Σ_{1-2} (cm^{-1})	Σ_t (cm^{-1})	χ
Group 1	Fuel	6.203E−3	1.780E−1	1.002E−2	1.966E−1	1.0
	Reflector	0.0	1.995E−1	2.188E−2	2.220E−1	
Group 2	Fuel	1.101E−1	1.089E−3	5.255E−1	5.962E−1	0.0
	Reflector	0.0	1.558E−3	8.783E−1	8.879E−1	

Table 4
Results of the simplified reactor core problem.

	K_{eff}	Average fast flux		Average thermal flux		CPU time (s)
		Fuel	Reflector	Fuel	Reflector	
Wavelet expansion	0.9919	0.0178	0.0029	0.0029	0.0035	366.9
Reference	0.9920	0.0178	0.0029	0.0029	0.0035	15.6
Error/%	0.01	0.10	0.17	−0.03	0.26	

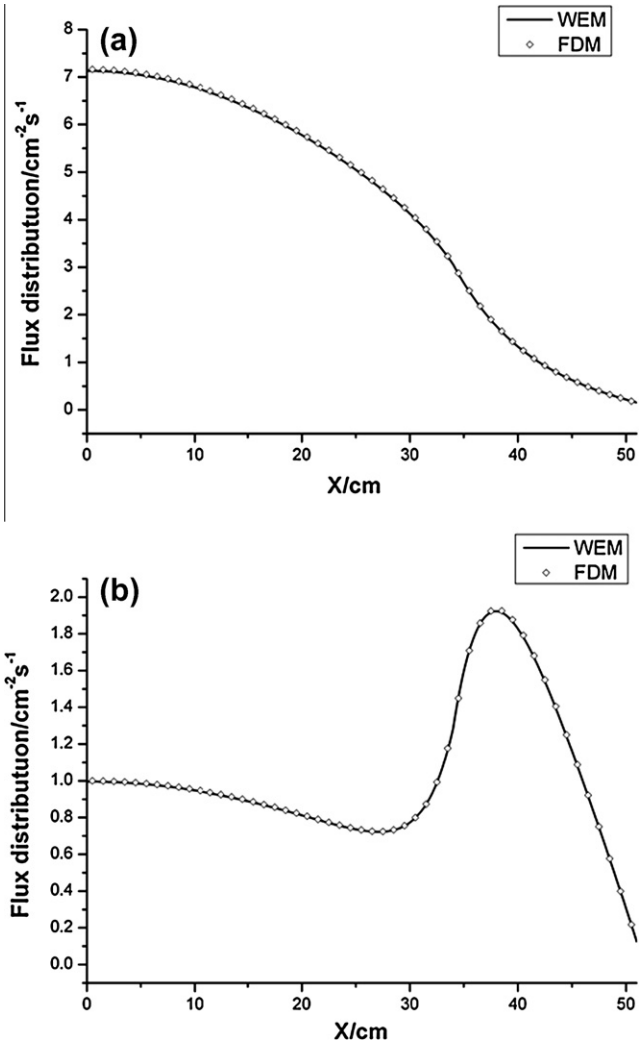

Fig. 12. Flux distribution in the simplified reactor core (a) for fast flux (b) for thermal flux.

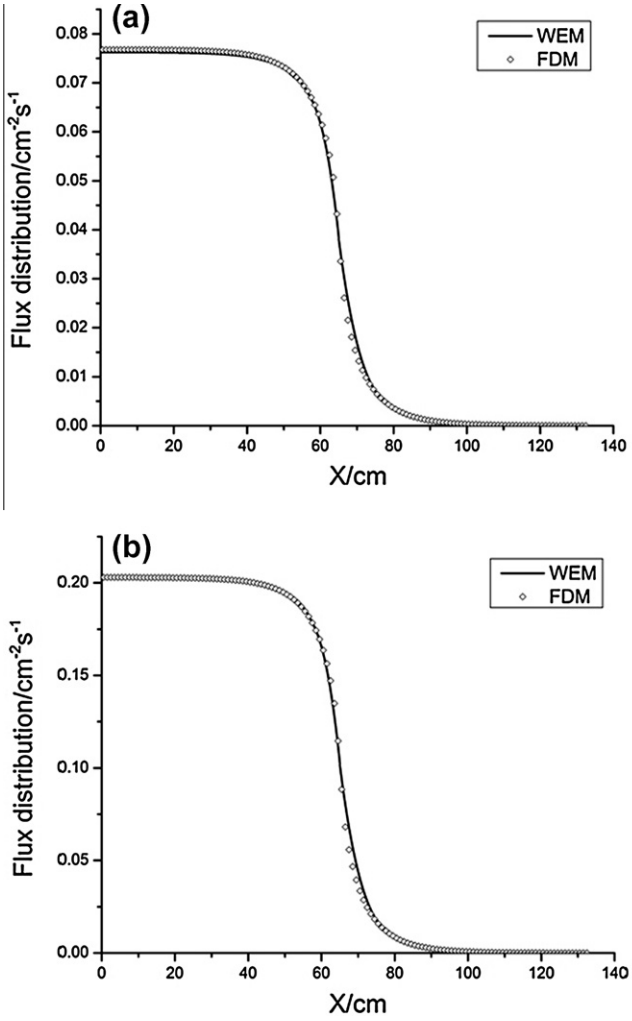

Fig. 14. Flux distribution in the deep penetration medium (a) for fast flux (b) for thermal flux.

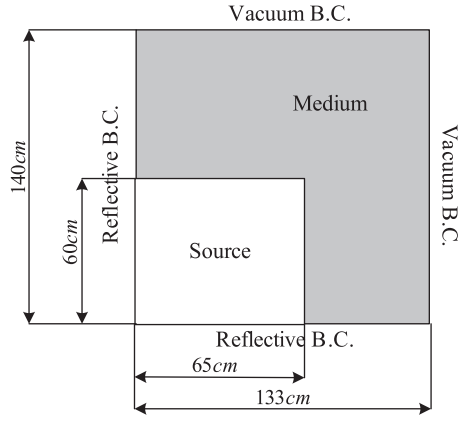

Fig. 13. Description of the deep penetration problem.

Table 5
Cross section of the deep penetration problem.

Group	S_g ($cm^{-3}\ s^{-1}$)	$\Sigma_{t,g}$ (cm^{-1})	$\Sigma_{s,g-1}$ (cm^{-1})	$\Sigma_{s,g-2}$ (cm^{-1})
1	0.0065	0.1011	0.0159	0.0234
2	0.0177	0.1085	0.0000	0.0125

The results of test problems so far have demonstrated that the new method is feasible and accurate in the neutron transport solution. It can directly simulate the continuous flux distribution in the medium. Generally, higher expansion order encourages better results but causes lower efficiency. In the problem suffering large graded distribution, the new method is powerful and efficient. For the high dimensional calculation, it is also accurate, but the efficiency is not so satisfying. It is due to the sharply increase of CPU time cost in solving the matrix formed by the tensor product expansion. Separation of variables may be a potentially effective approach, and the studies may be done in the future work.

Acknowledgements

This research was carried out under the financial support of the National Nature Science Foundation of China (Approved Number 11105104) and the Fundamental Research Funds of the Central University.

References

Buchan, A.G., Pain, C.C., et al., 2005. Linear and quadratic octahedral wavelets on the sphere for angular discretisations of the Boltzmann transport equation. Ann. Nucl. Energy 32 (11), 1224–1273.

Buchan, A.G., Pain, C.C., Eaton, M.D., et al., 2008a. Linear and quadratic hexahedral wavelets on the sphere for angular discretisations of the Boltzmann transport equation. Nucl. Sci. Eng. 159 (2), 127–152.

Buchan, A.G., Pain, C.C., Eaton, M.D., et al., 2008b. Chebyshev spectral hexahedral wavelets on the sphere for angular discretisations of the Boltzmann Transport Equation. Ann. Nucl. Energy 32 (6), 1098–1108.

Carron, I., 1999. Solving the transport equation with spline wavelets. Technical Report. Dept. of Nuclear Eng., Texas A&M University, College Station, Texas.

Cho, N.Z., Cao, L., 2006. Wavelet-theoretic method for solution of neutron transport equation. Transactions of the Korean Nuclear Society Spring Meeting, Chuncheon, Korea, May 25–26, 2006.

Cho, N.Z., Park, C.J., 1996. Wavelet theory for solution of the neutron diffusion equation. Nucl. Sci. Eng. 124, 417–430.

Cohen, A., Daubechies, I., Vial, P., 1993. Wavelets on the interval and fast wavelet transforms. Appl. Comput. Harmon. Anal. 1, 54–81.

Daubechies, I., 1992. Ten Lectures on Wavelets. SIAM, Philadelphia, PA.

Engle, W.W., 1973. A User's Manual for ANISN. USAEC Report KI-1693 (1967); ANISN-ORNL, A One-Dimensional Discrete Ordinates Transport Code. Oak Ridge National Laboratory Report CCC-254.

Issa, J.G., Riyait, N.S., Goddard, A.J.H., et al., 1986. Multigroup application of the anisotropic FEM code FELTRAN to one, two, three-dimensional and R–Z problems. Prog. Nucl. Eng. 18 (1), 251–264.

Lewis, E.E., Miller, W.F., 1984. Computational Method of Neutron Transport. John Wiley & Sons.

Nasif, H., Omori, R., Suzuki, A., 1999. Improved solution of the neutron diffusion equation using wavelet theory. J. Nucl. Sci. Technol. 36 (9), 839–842.

Nasif, H., Omori, R., Suzuki, A., et al., 2001. Wavelet-based algorithms for solving neutron diffusion equation. J. Nucl. Sci. Technol. 38 (3), 161–173.

Yang, W., WU, H., Zheng, Y., et al., 2010. Application of wavelets scaling function expansion method in resonance self-shielding calculation. Ann. Nucl. Energy 37, 653–663.

Zheng, Y., Wu, H., Cao, L., 2009. An improved three-dimensional wavelet-based method for solving the first-order Boltzmann transport equation. Ann. Nucl. Energy 36 (9), 1440–1449.

Zheng, Y., Wu, H., Cao, L., et al., 2010. Daubechies' wavelet method for angular solution of the neutron transport equation. Nucl. Sci. Eng. 164 (2), 87–104.